Nonlinear Sonic-Boom Propagation including the Asymmetric Effects

A. Ferri,* L. Ting,† and R.W. Lo‡
Division of Applied Science, New York University, N.Y.C., N.Y.

A numerical program is developed which takes into account the nonlinear effects of high Mach number, the entropy change across the shock, the entropy and enthalpy variations in the atmospheric layer and the gravitational effect. The program differs from the existing ones by accounting for nonaxisymmetric terms. The asymmetry can be caused by the geometry of the body, the lift, and also the fact that the variations in the atmospheric layer are two dimensional. Numerical results demonstrate that the influence of these asymmetric effects tends to lower the pressure signature.

I. Introduction

THE sonic boom induced by an airplane in supersonic flight was the primary cause of the ban on supersonic flight and the demise of our national SST program a few years ago. Recent commercial flights of Concorde point out that the advancement of technology cannot be stopped unilaterally. In order to reverse our public's opinion against SST, it is essential to show that we can design an SST which is financially attractive and produces a low boom over pressure at ground level, of the order of 1 psf or less, acceptable over populated areas. Many theoretical and experimental investigations[1-9] demonstrated adequately that for larger and slender airplanes, i.e., longer airplanes, the gound signature may not attain their far-field *N*-wave form. It may be possible to design an airplane weighing over 500,000 lbs with a low boom less than 1 psf by flying at higher Mach number[4-9] and at higher altitude (say over 80,000 ft). Additional references and a survey of present status in sonic boom research can be found in Refs. 8 and 9.

For an airplane flying at a moderate supersonic speed, the linearized theory is valid in the near-field. Whitham's theory[10] which makes second-order corrections to the outgoing characteristic lines and shock waves, yields accurate predictions for the pressure signature at ground level when the wing-body configuration is replaced by an equivalent axially symmetric body. Based upon Whithan's theory, there are two numerical programs[11,12] for the sonic boom analysis. The first program[11] is based on a uniform atmosphere and a correction factor for the reference pressure. The second program[12] is for nonuniform atmosphere. At high Mach number, say greater than 3, the nonlinear effects in the near field become more important.[5,7] At higher flight altitude, the variations of temperature and entropy of the atmosphere and the accumulation of the higher-order terms over long distance of wave propagation can be significant. Therefore, a third numerical program[7] was developed for the axisymmetric analysis including all the nonlinear terms in the governing equations and the nonuniformity of the atmosphere. The program is similar to the standard characteristic methods with a modification for the outgoing characteristics so that the line segment between two grid points is not a straight one. It is curved in a shape consistent with Whitham's theory, i.e., there are linear and square root terms. The same procedure is used for the shock shape. The characteristic equation is rearranged so that the left side is an exact differential of the invariant under Whithan's theory and the right side will be an order-of-magnitude smaller than that in a standard characteristic equation. Therefore, the step size along the outgoing characteristics can be increased to size of the body length in the far field. Numerical results from the nonlinear axisymmetric program were compared with those from the first two programs[11,12] in Ref. 7. The differences are significant for the location and strength of the rear shock. The difference in the strength of the bow shock increases as Mach number increases.

All three programs[7,11,12] are formulated for an axisymmetric or quasiaxisymmetric flowfield with the wing-body configuration replaced by an equivalent sysmmetric body. However, the real sonic boom problem is not axisymmetric because the nonuniformity in the atmosphere is two dimensional and the airplane configuration is not axisymmetric, in particular due to the life requirement. To check the degree of accuracy of the analyses based on the assumption of quasiaxisymmetry, we developed a numerical program which takes into account the asymmetric effects.

The new numerical program is basically an extrapolation method rather than a self-contained prediction method. It requires as input data a rather complete description of flowfield properties in the extreme near field of the aircraft; data such as might be supplied by wind-tunnel tests or by appropriate analytical methods when they become available. In this sense, the methods used for comparison are more complete. The method of Ref. 11 requires only an airplane area and lift distribution as input, but of course is applicable to the real atmosphere only through use of conversion factors obtained elsewhere. The method of Ref. 12 requires an *F* function as input (which may be generated by the method of

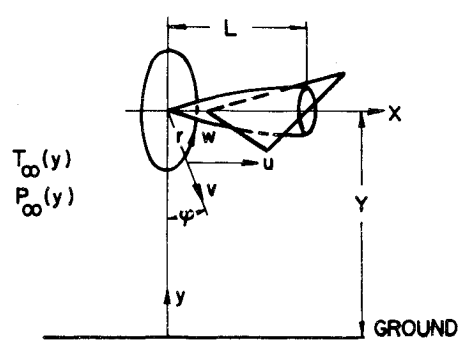

Fig. 1 Coordinate system for sonic-boom analysis.

Presented as Paper 76-587 at the 3rd AIAA Aero-Acoustics Conference, Palo Alto, Calif., July 20-23, 1976; submitted Aug. 12, 1976; revision received Feb. 23, 1977.

Index categories: Aircraft Noise, Aerodynamics (including Sonic Boom); Supersonic and Hypersonic Flow.

*Director of the Division of Applied Science and Astor Professor of Aerospace Science (Deceased Dec. 28, 1975). Fellow AIAA.

†Professor of Mathematics. Member AIAA.

‡Research Assistant, Division of Applied Science.

Ref. 11) and does account for the real atmosphere. The method of Ref. 7 requires the replacement of the wing-body configuration by an equivalent body of revolution. The various methods are thus not quite the direct competitors. Each has its own particular application and to some degree, as indicated above, the methods are complementary. The most important use of the method discussed here is likely to be in wind tunnel testing of proposed aircraft including low-boom designs. An extrapolation method such as this which permits consideration of flow asymmetries will allow close-in measurements for larger models. This would provide for more detail in modeling, more accuracy in measurement, and also would permit as-you-go tailoring of the model to better approach theoretical minimums.

II. The Analysis

For an airplane cruising at high altitude, the region of ground pressure signature, which is of prime interest, lies near the vertical plane of symmetry with respect to the airplane. In order to explain the approximations for the axisymmetric analysis and the corrections due to asymmetry near the vertical plane ($\psi=0$) we introduce cylindrical coordinates x, r, ψ with respect to the axis of the airplane (Fig. 1). The velocity components are u, v, w. Before writing down all the governing equations, we will make a simple count of the number of equations and unknowns. There are five equations; the continuity, energy, and three momentum equations for five unknowns, u, v, w, p, ρ. It is a three-dimensional problem involving variables (x,r,ψ). To simplify the notations, we introduce the symbol $\bar{}$ to denote the value in the vertical plane $\psi=0$, i.e.

$$\bar{u}(x,r)=u(x,r,0);\ \bar{u}_{\psi\psi}(x,r)=u_{\psi\psi}(x,r,0);\ \text{etc.} \tag{1}$$

In the plane $\psi=0$, the five governing equations reduce to four equations because the ψ-component of the momentum equations is an identity. Although $\bar{w}=0$, these four equations involve, $\bar{u}$, $\bar{v}$, $\bar{p}$, $\bar{\rho}$ and $\bar{w}_\psi/r$. The last one is neglected for large r in the quasiaxisymmetric theory. To include the asymmetric term $\bar{w}_\psi/r$ we are short of one equation. We will differentiate the ψ-component of the momentum equation with respect to ψ and the other four equations with respect to ψ twice and then set $\psi=0$. The results are five equations involving additional variables $\bar{u}_{\psi\psi}$, $\bar{v}_{\psi\psi}$, $\bar{p}_{\psi\psi}$, $\bar{\rho}_{\psi\psi}$, $\bar{w}_{\psi\psi\psi}/r$. We now have nine equations involving ten variables. Since the influence of $\bar{w}_{\psi\psi\psi}/r$ on the physical variables in the plane $\psi=0$, i.e., $\bar{u}$, $\bar{v}$, $\bar{p}$, $\bar{\rho}$, are of the order $1/r^3$ and both $\bar{w}_\psi$ and $\bar{w}_{\psi\psi\psi}$ are induced by the asymmetric terms, we introduce the closure condition

$$\bar{w}_{\psi\psi\psi}=-\bar{w}_\psi \tag{2}$$

which is valid if $\bar{w}$ behaves as $\sin\psi$ when the asymmetry is induced primarily by the lift. With the closure condition we now have nine governing equations in the plane $\psi=0$, for nine variables $\bar{u}$, $\bar{v}$, $\bar{p}$, $\bar{\rho}$, $\bar{w}_\psi$, $\bar{u}_{\psi\psi}$, $\bar{v}_{\psi\psi}$, $\bar{p}_{\psi\psi}$ and $\bar{\rho}_{\psi\psi}$ involving only two independent variables r and x.

Regarding conditions across a shock wave $x=f(r,\psi)$, we do not have to introduce any closure conditions. At $\psi=0$, the shock conditions yield the necessary number of equations for the jumps of $\bar{u}$, $\bar{v}$, $\bar{p}$, and $\bar{\rho}$. Now we will differentiate the shock conditions with respect to ψ and then set $\psi=0$, we obtain the necessary number of equations for the jumps of $\bar{u}_{\psi\psi}$, $\bar{v}_{\psi\psi}$, $\bar{p}_{\psi\psi}$, $\bar{\rho}_{\psi\psi}$, and $\bar{w}_\psi$.

The system of nine differential equations can be combined so that they can be integrated along unequal characteristics nets in a similar manner as in the axisymmetric cases.[7] The numerical program for the asymmetric analysis is then developed.

The method of this analysis differs from the method of perturbation from an axisymmetric flow; in the present method the characteristics in the plane $\psi=0$ are the true ones, while the latter correspond to the axisymmetric flow only.

This analysis is based on the consideration of large r, i.e., the far field, and cannot be applied to the neighborhood of the wing-body configuration. The numerical program is applicable at a distance from the airplane. The boundary data required for the program (say at $r=$ body length) have to be furnished by a different source, e.g., a three-dimensional analysis of the near field or wind-tunnel test data. The present analysis in turn provides the quantities which should be measured in the wind tunnel in order to carry out the far-field analysis. Details of the analysis are described in the next two subsections.

A. Governing Differential Equations

The governing equations for the inviscid flowfield, including the gravitational terms and the variation in total energy due to the nonuniformity of the atmosphere, are

$$\nabla\cdot v+v\cdot(\rho^{-1}\nabla\rho)=0 \tag{3}$$

$$(v\cdot\nabla)v=-\rho^{-1}\nabla p+g \tag{4}$$

$$v\cdot\nabla H=0 \tag{5}$$

where

$$p=\rho RT=\rho a^2/\gamma \tag{6}$$

$$H=a^2(\gamma-1)^{-1}+V^2/2+\int g\,dy \tag{7}$$

g is the standard gravity and the y-axis points in the vertical direction. For the convenience of numerical computation later on, the pressure and density variables are eliminated from Eqs. (3) and (4), and the results are

$$\nabla\cdot v-a^{-2}v\cdot\nabla(V^2/2)=(v\cdot g)/a^2 \tag{8}$$

$$(\nabla\times v)\times v=T\nabla S-\nabla H \tag{9}$$

The component of Eq. (8) along the streamline yields

$$v\cdot\nabla S=0 \tag{10}$$

Ahead of the front shock wave, the velocity is uniform with velocity $U_\infty i$; the temperature $T_\infty(y)$ and pressure $P_\infty(y)$ are given functions of the altitude y, fulfilling the hydrostatic equilibrium condition

$$[\rho_\infty(y)]^{-1}(dp_\infty/dy)=-g \tag{11}$$

For an airplane flying at a constant altitude Y, it is convenient to introduce cylindrical coordinates x, r, ϕ with velocity components u, v, w (Fig. 1) with

$$y=Y-r\cos\psi \tag{12}$$

$$\nabla=\hat{i}(\partial/\partial x)+\hat{r}(\partial/\partial r)+\hat{\psi}(r^{-1}\partial/\partial\psi) \tag{13}$$

In the vertical plane of symmetry ($\psi=0$), the circumferential component w vanishes; however, the circumferential derivative of w does not. The circumferential derivatives of u, v, H, and S vanish at $\psi=0$ because of symmetry. The governing equations (8, 9, 5 and 10) reduce to

$$\left(1-\frac{\bar{u}^2}{\bar{a}^2}\right)\bar{u}_x-\frac{\bar{u}\bar{v}}{\bar{a}^2}(\bar{u}_r+\bar{v}_x)+\left(1-\frac{\bar{v}^2}{\bar{a}^2}\right)\bar{v}_r=-\frac{\bar{v}}{r}-\frac{g\bar{v}}{\bar{a}^2}-\frac{\hat{w}}{r} \tag{14}$$

$$\bar{q}^2(\bar{v}_x-\bar{u}_r)=-\bar{q}\frac{\partial\bar{H}}{\partial n}+\bar{q}\bar{T}\frac{\partial\bar{S}}{\partial n} \tag{15}$$

$$\left(\bar{u}\frac{\partial}{\partial x}+\bar{v}\frac{\partial}{\partial r}\right)\bar{H}=\frac{\partial\bar{H}}{\partial\sigma}=0 \tag{16}$$

$$\left(\bar{u}\frac{\partial}{\partial x}+\bar{v}\frac{\partial}{\partial r}\right)\bar{S}=\frac{\partial\bar{S}}{\partial\sigma}=0 \tag{17}$$

where $\hat{w}(x,r)=\bar{w}_\psi$, $\bar{q}^2=\bar{u}^2+\bar{v}^2$, $\bar{q}\partial/\partial n=\bar{u}\partial/\partial r-\bar{v}\partial/\partial x$; σ is the arc length along a streamline. In the vertical plane of symmetry, the asymmetry effect appears only through the term $\hat{w}/r$ in the continuity equation (14). If we ignore $\hat{w}/r$ on the grounds of large r, we arrive at the axisymmetric theory.

Since the ψ-component of Eq. (9) on the plane $\psi=0$ is a trivial equation, it is differentiated with respect to ψ and then set $\psi=0$. The result is a differential equation for $\hat{w}$

$$\bar{q}\frac{\partial\hat{w}}{\partial\sigma}=[-\bar{v}\hat{w}-\bar{H}+\bar{a}^2\bar{S}/(\gamma R)+\bar{u}\bar{u}+\bar{v}\bar{v}]/r \tag{18}$$

Unfortunately, we have four additional unknowns $\bar{u}$, $\bar{v}$, $\bar{H}$, $\bar{S}$, where $(\sim)$ represents the second ψ derivative of the quantity at $\psi=0$, e.g., $\bar{u}(x,r)=u_{\psi\psi}(x,r,0)$.

Since the first ψ derivatives of the remaining equations of Eqs. (8, 9, 5 and 10) are trivial at $\psi=0$, their second ψ derivatives at $\psi=0$ yield

$$(1-\bar{u}^2/\bar{a}^2)\bar{u}_x-(\bar{u}\bar{v}/\bar{a}^2)(\bar{u}_r+\bar{v}_x)+(1-\bar{v}^2/\bar{a}^2)\bar{v}_r=$$
$$-\hat{w}_{\psi\psi}/r-\bar{v}/r+\bar{a}^{-2}\Big\{\bar{q}\Big(\bar{u}\frac{\partial\bar{u}}{\partial\sigma}+\bar{v}\frac{\partial\bar{v}}{\partial\sigma}\Big)$$
$$+2\hat{w}\Big[g+\bar{q}\frac{\partial\hat{w}}{\partial\sigma}+(\bar{u}\bar{u}+\bar{v}\bar{v}+\hat{w}^2)/r\Big]$$
$$+g(\bar{v}-\bar{v})+\Big(\bar{u}\frac{\partial}{\partial x}+\bar{v}\frac{\partial}{\partial r}\Big)\bar{q}^2/2-(\bar{a}^2/\bar{a}^2)^2\Big(\bar{q}^2\frac{\partial\bar{q}}{\partial\sigma}-\bar{v}g\Big)\Big\} \tag{19}$$

$$\bar{q}^2(\bar{u}_r-\bar{v}_x)=-\bar{q}(\partial\bar{H}/\partial n)+\bar{q}^3(\partial\bar{S}/\partial n)/(\gamma RM^2)$$
$$-2\hat{w}(\bar{u}\bar{v}-\bar{v}\bar{u})/r+2\bar{q}\hat{w}(\partial\hat{w}/\partial n)-2\hat{w}^2\bar{u}/r$$
$$+(\bar{u}\bar{u}+\bar{v}\bar{v})(\bar{v}_x-\bar{u}_r)-\bar{a}^2\bar{q}(\partial\bar{s}/\partial n)/(\gamma R) \tag{20}$$

$$\bar{q}(\partial\bar{H}/\partial\sigma)=-[\bar{u}(\partial/\partial x)+\bar{v}(\partial/\partial r)]\bar{H}-2\hat{w}\bar{H}/r \tag{21}$$

$$\bar{q}(\partial\bar{S}/\partial\sigma)=[\bar{u}(\partial/\partial x)+\bar{v}(\partial/\partial r)]\bar{S}-2\hat{w}\bar{S}/r \tag{22}$$

The first set of four equations (14-17) and the second set of five equations (18-22) would form a closed system for the unknowns $\bar{u}$, $\bar{v}$, $\bar{H}$, $\bar{S}$, and $\hat{w}$, $\bar{u}$, $\bar{v}$, $\bar{H}$, $\bar{S}$ if Eq. (19) did not contain a new unknown $\hat{w}_{\psi\psi}$ which is $w_{\psi\psi\psi}(x,r,0)$. A closure condition is introduced,

$$\hat{w}_{\psi\psi}=-\hat{w} \tag{23}$$

The condition can be justified on the assumption that the basic contribution of asymmetry is first harmonic in ψ, i.e., $w(x,r,\psi)\sim\bar{w}(x,r)\sin\psi$. This is logical because, with the asymmetry due to lift and that due to two-dimensional nonuniformity in the atmosphere, there are predominantly first harmonic terms in ψ. With the closure condition of Eq. (23), Eqs. (14-22) form the complete system for the nine unknowns, $\bar{u}$, $\bar{v}$, $\bar{H}$, $\bar{S}$ and $\hat{w}$, $\bar{u}$, $\bar{v}$, $\bar{H}$, $\bar{S}$.

An iterative procedure for the numerical integration of those nine equations will be described. The first four equations can be considered as four equations $\bar{u}$, $\bar{v}$, $\bar{H}$, $\bar{S}$ when $\hat{w}$ is assumed to be assigned. In that case they can be integrated in the same manner as in the axisymmetric problem. That is, we recombine Eqs. (14) and (15) to two equations to be integrated along the two characteristics in the plane $\psi=0$ for the determination of the new characteristic grid point and the values for $\bar{u}$ and $\bar{v}$ or their equivalent variables, say M and θ, and the other two equations (16) and (17) are integrated along the streamlines for the value of $\bar{H}$ and $\bar{S}$. When the values of $\bar{u}$, $\bar{v}$, $\bar{H}$ and $\bar{S}$ at the new grid point converge to their final values corresponding to an assigned value of $\hat{w}$, which will be equal to the value at the nearest grid point for the first cycle of iteration, we proceed to integrate Eqs. (18-22) for the values of the asymmetric variables at the new grid point. We note that the differential operators on $\bar{u}$ and $\bar{v}$ on the left sides of Eqs. (19) and (20) are the same as those for $\bar{u}$ and $\bar{v}$ in Eqs. (14) and (15). They will be recombined in the same manner into two equations to be integrated along the two characteristic lines for the determination of $\bar{u}$, $\bar{v}$ at the new grid point. Eqs. (18-21, 22) will be integrated along the streamline for $\hat{w}$, $\bar{H}$ and $\bar{S}$. Thus one cycle of the iteration process is completed. With the new value for $\hat{w}$ we start the next cycle until the differences of the values between two cycles are insignificant.

B. The Shock Conditions

We will develop the shock conditions across an embedded shock front $x=f(r,\psi)$. The quantities ahead and behind the shock will be designated by the subscripts 1 and 2 respectively. The conditions across the bow shock can be obtained when the quantities ahead of the shock, i.e., with subscript 1, are replaced by the undistrubed flow quantities ahead of the bow shock.

The conservation conditions across the shock front are:

Mass

$$\rho_1[u_1-v_1f_r-w_1f_\psi/r]=m=\rho_2[u_2-v_2f_r-w_2f_\psi/r] \tag{24}$$

Momentum components

$$mu_1+p_1=mu_2+p_2 \tag{25}$$

$$u_1f_r+v_1=u_2f_r+v_2 \tag{26}$$

$$u_1f_\psi/r+w_1=u_2f_\psi/r+w_2 \tag{27}$$

Energy

$$u_1^2+v_1^2+w_1^2+2\gamma RT_1/(\gamma-1)$$
$$=u_2^2+v_2^2+w_2^2+2\gamma RT_2/(\gamma-1) \tag{28}$$

In the vertical plane of symmetry ($\psi=0$) these conditions become:

$$\bar{\rho}_1[\bar{u}_1-\bar{v}_1\bar{f}_r]=\bar{m}=\bar{\rho}_2[\bar{u}_2-\bar{v}_2\bar{f}_r] \tag{29}$$

$$\bar{m}\bar{u}_1+\bar{p}_1=\bar{m}\bar{u}_2+\bar{p}_2 \tag{30}$$

$$\bar{u}_1\bar{f}_r+\bar{v}_1=\bar{u}_2\bar{f}_r+\bar{v}_2 \tag{31}$$

$$\bar{u}_1^2+\bar{v}_1^2+2\gamma\bar{p}_1([\bar{\rho}_1(\gamma-1)]$$
$$=\bar{u}_2^2+\bar{v}_2^2+2\gamma\bar{p}_2/[\bar{\rho}_2(\gamma-1)] \tag{32}$$

while Eq. (27) becomes an identity. These four equations are the standard oblique shock equations. We note that $\bar{f}_r=f_r(r,0)=\cot(\bar{\beta}+\bar{\theta}_1)$ where $\bar{\beta}$ is the shock angle with respect to the flow direction ahead of the shock.

It should be pointed out here that for weak shocks these four equations in the first approximation, become four homogeneous equations for the differences $\bar{u}_2-\bar{u}_1$, $\bar{v}_2-\bar{v}_1$, $\bar{p}_2-\bar{p}_1$ and $\bar{\rho}_2-\bar{\rho}_1$. The determinant of the linear equation vanishes as the shock angle $\bar{\beta}$ approaches the Mach angle.

We could proceed to establish the shock conditions for the asymmetric quantities in the same manner as for the differential equations, i.e., we differentiate Eqs. (24, 25, 26, 28) with respect to ψ twice on the surface $x=f(r,\psi)$ and Eq. (27) with respect to ψ once and then set $\psi=0$. The last equation becomes

$$\bar{u}_1\bar{f}+\hat{w}_1r=\bar{u}_2\bar{f}+\hat{w}_2r \tag{33}$$

where $\bar{f}(r) = f_{\psi\psi}(r,0)$. It can be considered as an equation for $\hat{w}_{2\psi}$ while the other four equations are the equations for the second ψ derivative of u_2, v_2, p_2, and ρ_2 at $\psi = 0$. Unfortunately, for weak shocks the determinant of the four equations are the same as that for the weak oblique shock mentioned before, therefore, the iteration scheme will involve the complications of ratios of small numbers and leads to inaccuracy and nonconvergence. To avoid this difficulty we should recombine the basic equations before differentiations with respect to ψ so as to cancel out analytically a common factor which vanish for zero shock strength.

After the elimination of p and ρ, the shock equations (24-28) become:

$$(u_2 - u_1) + \frac{RT_2}{Q_2} - \frac{RT}{Q_1} = 0 \tag{34}$$

$$(u_2 - u_1) f_r + (v_2 - v_1) = 0 \tag{35}$$

$$(u_2 - u_1) f_\psi / r + (w_2 - w_1) = 0 \tag{36}$$

$$(u_2 + u_1)(u_2 - u_1) + (v_2 + v_1)(v_2 - v_1) + (w_2 + w_1)(w_2 - w_1) + 2\gamma R(T_2 - T_1)/(\Gamma - 1) = 0 \tag{37}$$

where $Q_j = u_j - v_j f_r - w_j f_\psi / r$ for $j = 1,2$. Eq. (34) can be rewritten as

$$(u_2 - u_1)[Q_1 Q_2 (RT_1)^{-1} - 1] + (v_2 - v_1) f_r + (w_2 - w_1) f_\psi / r = 0 \tag{38}$$

After the elimination of v_2, v_1, $w_2 - w_1$ and $T_2 - T_1$ we get

$$(u_2 - u_1)\{Q_2 Q_1 - RT(1 + f_r^2 + f_\psi^2/r^2) - (\gamma - 1) Q_1 (Q_1 + Q_2)/(2\gamma)\} = 0$$

Since $u_2 - u_1 \neq 0$, we have

$$2\gamma R T_1 (1 + f_r^2 + f_\psi^2/r^2) = (\gamma + 1) Q_1 Q_2 - (\gamma - 1) Q_1^2 \tag{39}$$

This equation can be used to replace any one of the shock conditions. Since Eqs. (39), (35), and (36) involves only u_2, v_2, and w_2, they form a complete set of shock conditions. To obtain the shock conditions for the asymmetric variables, we differentiate Eqs. (35) and (39) with respect to ψ twice on the shock surface $x = f(r,\psi)$ and the set $\psi = 0$. The results are:

$$(\tilde{u}_2 - \tilde{u}_1) \bar{f}_r + \tilde{v}_2 - \tilde{v}_1 + (\bar{u}_2 - \bar{u}_1) \bar{f}_r + [(\tilde{u}_{2x} - \tilde{u}_{1x}) \bar{f}_r + \bar{v}_{2x} - \bar{v}_{1x}] \bar{f}_r = 0 \tag{40}$$

and

$$2\Gamma R(\bar{T}_1 + \bar{T}_{1x} \bar{f})(1 + \bar{f}_r^2) + 4\gamma R \bar{T}_1 (\bar{f}_r \bar{f}_r + 2\bar{f}^2/r^2) = (\gamma + 1)(\tilde{Q}_1 \bar{Q}_2 + \tilde{Q}_2 \bar{Q}_1) - 2(\gamma - 1) \tilde{Q}_1 \bar{Q}_1 \tag{41}$$

where

$$\bar{Q}_j = \bar{u}_j - \bar{v}_j \bar{f}_r$$

$$\tilde{Q}_j = \tilde{u}_j - \bar{v}_j \bar{f}_r - \bar{v}_j \bar{f}_r + (\bar{u}_{jx} - \bar{v}_{jx} \bar{f}_r) \bar{f}$$

for $j = 1,2$. These two equations together with Eq. (33) are the governing shock conditions for the asymmetric variables $\tilde{u}_2$, $\tilde{v}_2$, $\hat{w}_2$ and the shock shape $\bar{f}$. Of course, another equation relating $\tilde{u}_2$ and $\tilde{v}_2$ will be supplied by the equation along the outgoing characteristic line.

As we have mentioned before, the shock equations (29-32) for the variables in the plane $\psi = 0$ are uncoupled with those for the asymmetric variables. However, they are coupled indirectly because of the appearance of $\hat{w}_2$ in the outgoing characteristic equation. The iteration procedure for a new shock point will be similar to that for a new characteristic point. That is, we will first assign the value of $\hat{w}$ and determine the shock position and the variables in plane $\psi = 0$ as an axisymmetric problem. We will then use the asymmetric shock conditions (33, 40, 41) together with the equation for the asymmetric variables along the outgoing characteristics to determine $\tilde{u}_2$, $\tilde{v}_2$, $\hat{w}_2$ and $\bar{f}$. Thus we complete one cycle of iteration. Using the new values for $\hat{w}_2$ we proceed to the next cycle until the differences between the results of two cycles are insignificant.

The computation for the formation of an embedded shock is accomplished by calling the subroutine for characteristic points and then the subroutine for embedded shock. Since these subroutines include the computation for asymmetric terms, so does the computation for the formation of an embedded shock.

III. Numerical Results and Discussion

A numerical program for the asymmetric analysis outlined in the preceding section has been completed by F. Kung. The numerical program requires input data at a finite distance from the body, say one body length. These data can be obtained from a full three-dimensional analysis of the wing-body configuration or from the experimental data. In order to show the significance of the asymmetric effect, we prepared our input data as follows: and equipment axisymmetric area distribution representing the wing-body volume and lift contributions is chosen in the same way as in the existing procedures[10,11,7] for sonic-boom analysis. Our nonlinear axisymmetric program[7] is employed to give the ground signature and to create the data at one body length for the variables in the plane of symmetry. The asymmetric data, i.e., the circumferential derivatives, are evaluated from the linearized theory when a lift disttribution along the axis is assigned. The location of the lift distribution at one body length distance is corrected from the linear theory by following the nonlinear outgoing characteristic line. In this paper a reflection factor of 1.8 was used in obtaining the ground level signature.

Figure 2 shows the pressure signatures from different numerical programs namely, the uniform atmospheric program and the real atmospheric program based on Whitham theory, the nonlinear azisymmetric program[7] and the present analysis at $M_\infty = 4$ flying at 80,000 ft. The equivalent area distributions are shown in Fig. 3. The combined volume and lift distributions are given by a cone-parabolic body of length 300 ft while the base area is the maximum area of 596 sq. ft for a 15 ft cone with a half angle of 5°. The length of the body and the length of the cone will remain the same for all the numerical examples in this paper. The lift distribution for case B has a maximum chord length of 80% body length. The sectional lift increases linearly from the leading edge at 20% of the body length to the maximum

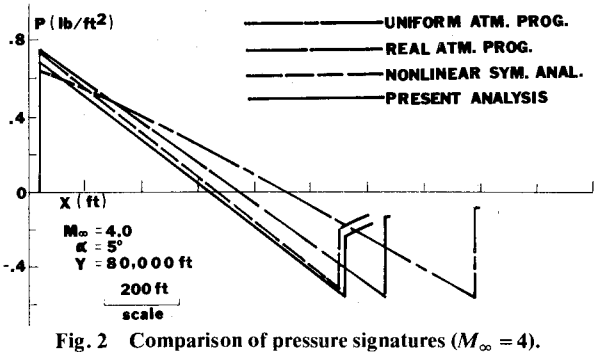

Fig. 2 Comparison of pressure signatures ($M_\infty = 4$).

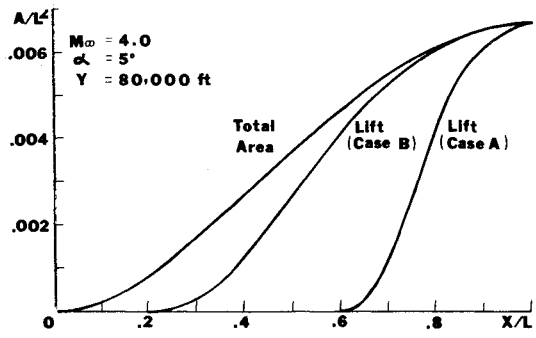

Fig. 3 Equivalent body shapes ($\alpha = 5°$).

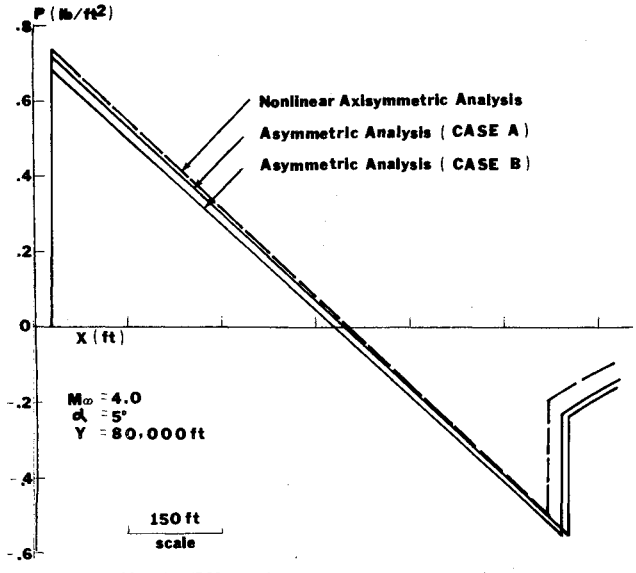

Fig. 4 Effect of different lift distributions.

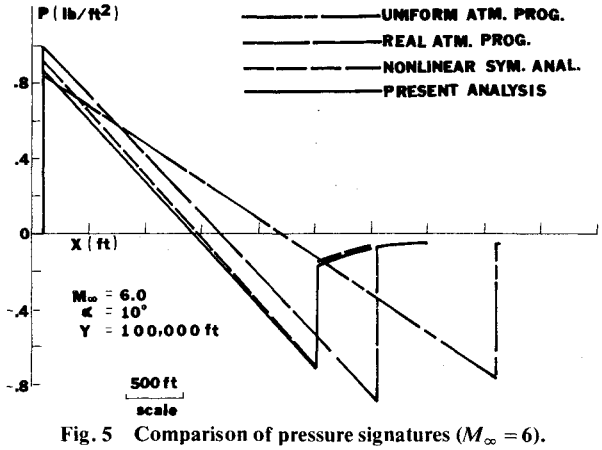

Fig. 5 Comparison of pressure signatures ($M_\infty = 6$).

value at 1/3 of the chord and then decreases linearly to zero at the trailing edge. The total lift corresponding to the maximum area of 596 sq. ft is 219,000 lbs. For case A the chordwise lift distribution is similar to that of B, but the total chord length is reduced to 40% and begins at 60% of the body length. The total lift remains the same.

Figure 2 shows that there is a significant difference between the two methods based on Whitham theory for uniform and real atmosphere and with the nonlinear axisymmetric theory especially for the rear shock. These results were reported in Ref. 7. The asymmetric effect reduced the pressure signature from the axisymmetric analysis by 15%.

Figure 4 shows the effect of lift distributions. As expected, when the lift distribution is shifted backward from 20% to

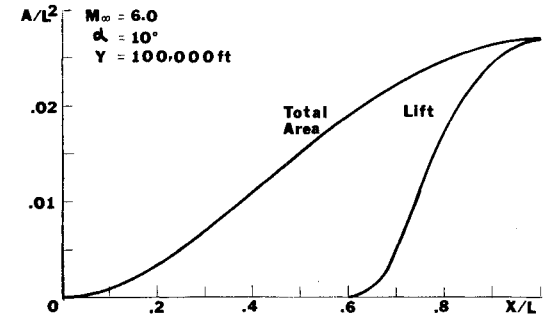

Fig. 6 Equivalent body shapes ($\alpha = 10°$).

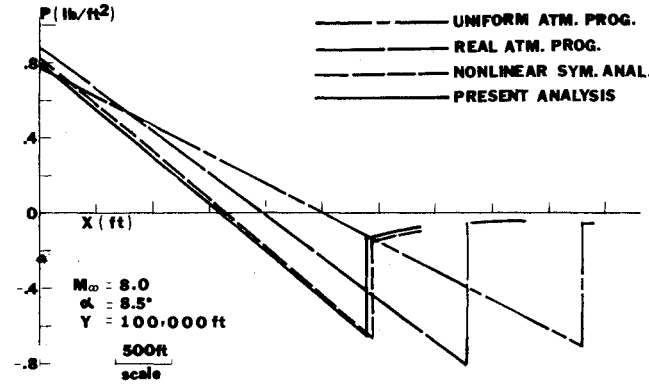

Fig. 7 Comparison of pressure signatures ($M_\infty = 8$).

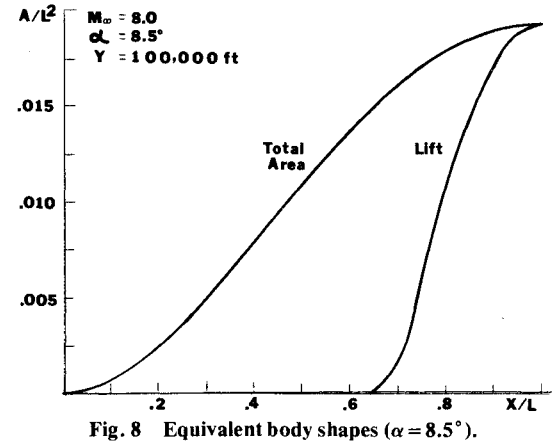

Fig. 8 Equivalent body shapes ($\alpha = 8.5°$).

60% of the body length the asymmetric corrections become much smaller.

Figure 5 shows the pressure signatures from the four numerical programs for $M_\infty = 6$ flying at 100,000 ft. The equivalent area distributions are shown in Fig. 6. The half cone angle is 10° and the maximum area is 2420 sq. ft corresponding to a total lift of 531,000 lbs. Their differences are quantitatively the same as in Fig. 2, although the maximum load is more than doubled. The maximum boom is only about 0.9 lbs/sq. ft. The lift distribution shown in Fig. 6 is similar to case A of Fig. 4, i.e., it begins at 60% of the body length. The reduction in the bow shock strength is almost 7%. The interference is stronger because of larger Mach number and total area so that the characteristic line from the leading edge is now only slightly behind the bow shock at one body length away.

Figure 7 shows the pressure signatures from four numerical programs for $M_\infty = 8$ flying at 100,000 ft. The equivalent area distributions are shown in Fig. 8. The half cone angle is 8.5° and the maximum area is 1740 sq. ft corresponding to total lift of 505,000 lbs. Again we see similar differences between them. The maximum boom is only about 0.8 lbs/sq. ft.

From these numerical examples, we show that we can design an SST weighing 500,000 lbs with maximum boom less than 1 lb/sq. ft and also confirm that asymmetric effects due to lift do reduce the theoretical value predicted by the axisymmetric theory. We know that there are other asymmetric effects in a wing-body configuration, namely the spanwise distribution of volume and lift. Their effects represent basically the second harmonic term in the circumferential variable ψ and are not included in the present analysis. Efforts are being made to include corrections due to those asymmetric affects in our theoretical predictions.

Acknowledgments

The work reported herein was supported by NASA under Grant NGL-33-016-119. The authors wish to thank F. Kung for her effort in developing the numerical program.

References

[1]McLean, F. E., "Some Nonasymptotic Effects on Sonic Boom of Large Airplanes," NASA TN D-2877, 1965.

[2]Ferri, A. and Ismail, A., "Effects of Lengthwise Lift Distribution on Sonic Boom of SST Configurations," *AIAA Journal*, Vol. 7, Aug. 1969 pp. 1538-1541.

[3]George., A.R., "Lower Bounds for Sonic Booms in the Mid-field," *AIAA Journal*, Vol. 7, Aug. 1969, pp. 1542-1545.

[4]Ferri, A., Wang, H.C., and Sorensen, H., "Experimental Verification of Low Sonic Boom Configuration," NASA CR-2070, June 1972.

[5]Landahl, M., Ryhming, I., Sorensen, H., and Drougge, G., "A New Method for Determining Sonic Boom Strength from Near-Field Measurements," *NASA Third Conference on Sonic Boom Research*, NASA SP-255, Oct. 1970, pp. 285-295.

[6]Carlson, H.W., Barger, R.L., and Mach, R.J., "Application of Sonic Boom Minimization Concepts in SST Design," NASA TN-D-7218, June 1973.

[7]Ferri, A., Siclari, M., and Ting, L., "Sonic Boom Analysis for High Altitude Flights at High Mach Numbers," *AIAA Progress in Astronautics and Aeronautics: Acoutics: Fan, STOL, and Boundary Layer Noise; Sonic Boom; Aeroacoustics Instrumentation*, Vol. 38, Editor: Henry T. Nagamatsu, Associate Editors: Jack V.O'Keefe and Ira R. Schwartz, MIT Press, Cambridge, Mass., 1975, pp. 301-320.

[8]Seebass, A.R. and George, A.R., "Design and Operation of Aircraft to Minimize Their Sonic Boom," *Journal of Aircraft*, Vol. 11, Sept. 1974, pp. 509-517.

[9]Darden, C.M., "Sonic Boom Theory: Its Status in Prediction and Minimization," AIAA Paper 76-1, Washington, D.C., 1976; to be published in *Journal of Aircraft*..

[10]Whithan, G.B., "The Flow Pattern of a Supersonic Projectile," *Communication in Pure and Applied Mathematics*, Vol. 5, Aug. 1952, pp. 301-349.

[11]Carlson, H.W., "Comparison of Sonic Boom Theory with Wind Tunnel and Flight Measurements," NASA TR-R-213, 1964.

[12]Hayes, W.D., Haefile, R.C., and Kulsrud, H.W., "Sonic Boom Propagation in a Stratified Atmosphere with Computer Program," NASA CR-1299, 1969.

[13]Kung, F., "Numerical Program for Sonic Boom Analysis-Nonlinear with Asymmetric Correction Due to Lift," Division of Applied Science/New York University Rept. AA76-11, June 1976.